

Article

Micromechanism of Cold Deformation of Two Phase Polycrystalline Ti-Al Alloy with Void

Ruicheng Feng^{1,2} ; Maomao Wang^{1,*} ; Haiyan Li^{1,*}; Yongnian Qi¹; Qi Wang¹; Zhiyuan Rui^{1,2}

¹ School of Mechanical and Electronical Engineering, Lanzhou University of Technology, Lanzhou 730050, China; frcly@163.com(R.F.); 15620864891@163.com(M.W.); y5217@163.com(H.L.); 13893591491@163.com(Y.Q.); 18350122524@163.com(Q.W.); zhiy_rui@163.com(Z.R.)

² State Key Laboratory of Advanced Processing and Recycling of Non-ferrous Metals, Lanzhou University of Technology, Lanzhou 730050, China

* Correspondence: 15620864891@163.com; y5217@163.com

Version December 25, 2018 submitted to Materials

Abstract: Cold deformation behavior of polycrystalline metallic material is affected by intrinsic defects such as dislocation, void, inclusion etc. Existing studies on $\alpha_2(\text{Ti}_3\text{Al})+\gamma(\text{TiAl})$ two phase Ti-Al alloy cover about deformation behavior mainly on macro scale. This paper focuses on the cold deformation mechanism of two phase Ti-Al alloy at micro scale, and the role of void in deformation process. Molecular dynamics simulations were performed to study the evolution of micro structure of material under uniaxial tension. Interaction between spherical nano void with different size and position was also examined in the simulation. The results show that (1) In elastic stage, deformation of the two phase is coordinated, but Ti_3Al is more deformable;(2) In plastic stage, γ phase is the major dislocation source in two phase alloy; (3) void detracts the strength of the two phase alloy, while the position of void affect the degree of this subtraction, voids located at the boundary of α_2/γ phase have significant detraction to strength.

Keywords: two phase Ti-Al alloy; void; molecular dynamics; cold deformation

1. Introduction

Titanium aluminum based intermetallic alloys are promising high temperature structural materials because of their great corrosion resistance and strength at high temperature. Compared with ~~nickle nickel~~ based alloy, Ti-Al based alloys have lower density ~~and are pron to be utilized, it can be used~~ in combustion engine, turbine, and other components working at high temperature from 500 °C to 900 °C [1]. The performance of inner combustion engine with components made of Ti-6Al-4V was improved 20% because the weight of components decreased from 30% to 40% [2]. With the advancement of non-ferrous metallurgy, Ti-Al based alloy components have better economic efficiency than ever before. Ti-Al based alloys have good prospects for applications in aerospace and automobile industry. Poor ductility of Ti-Al alloy at room temperature strongly affects the safety of structures like turbo of aircraft engine and combustion generator [3].

Deformation phenomena of Ti-Al alloys have been widely studied in order to overcome the problems associated with the ~~limited poor~~ ductility and damage tolerance. Much of the work has been performed on single phase γ -TiAl alloys, Ti_3Al alloys, and polysynthetically twinned crystals(PTC)[4]. ~~Experiments reveals that the dominant deformation mode in Ti_3Al at low temperature is slip activity without any twinning, and fracture type is cleavage[5]. Around 1990s, experimental studies on the two phase lamellae Ti-Al alloys show that mechanical twin and glide of dislocation are major sources of deformation[6–8].~~ Rapture failure at the macroscopic scale can be attributed to abrupt nucleation, growth and propagation of cracks, but at the microscopic scale, ~~defects are initially formed in the~~

casting process, such as voids and inclusions [9]. Mess research cover a wide range of factors such as alloy composition, microstructure and deformation temperature, some reports come up with the idea that two phase titanium aluminum alloys with proper phase distribution and grain size exhibit better mechanical performance compared with monolithic constituents γ (TiAl) and α_2 (Ti₃Al) alloy [10]. In situ experiments have shown that TiAl and Ti₃Al in two phase alloy exhibit different properties comparing in single phase alloys[11], void can be arose due to specific volume differences induced by precipitation, different thermal expansion or shrinkage upon heating or cooling the specimen. It has been known that nucleation, growth and coalescence of voids are deemed as the primary mechanism of ductile material fracture, in which void growth is particularly important [12]. The initiation of crack at microscopic scale is a dynamic process, which results in difficulties on study of mechanism about deformation and cracking, these defects are known playing a fundamental role in the deformation of materials. Multiscale method has been applied to study deformation behavior of polycrystal with single aluminum [13] and titanium element respectively [14]. It's necessary to carefully examine the revolution of defects and its influence on the fracture process at atomic scale.

The effect of void is another great concern about properties and deformation mechanism of TiAl alloy. Therefore, it is necessary to study the deformation response of intermetallics structural materials with the consideration of microstructure evolution. Previous study on void growth in single crystal γ -TiAl reveals that void with high volume fraction detracts yield strength [9,15]. Evolution of void in ductile polycrystalline was studied in nanoscale with molecular dynamics(MD) simulations, [16,17], voids inside material are sources of dislocation and affects the properties of materials differently because of differences in size and position. The deformation and fracture mechanisms in the duplex microstructure are plasticity induced grain boundary decohesion and cleavage, while those in the lamellar micro-structure are interface delamination and cracking across the lamellar [9]. It reveals that existence of voids alone may contribute to strain hardening because they are barriers to dislocation movement in ductile fcc structure metal[18]. However, few literature covers about deformation mechanism of two phase Ti-Al alloy and the role of void in atomic scale. Defects are inevitable as micro-pores and loosen from casting, and in the actual work environment with radiation. A lot of work carried out on the effect of various defects on the behavior of different materials, showing that point defects may affect the properties of materials greatly. The mechanical performance of irradiated copper is affected by the interaction between irradiation and dislocation [19]. Vacancy concentration in single crystal and polycrystal Fe-40 at. Al bulk results in an increase of strength [20]. Ti-Al alloy is a type of typical brittle material, thus it can be assumed that its properties are sensitive to the existence of void. Surface defects such as small notches can cause low and high cycle fatigue strength of the Ti-47Al-2W-0.5Si alloy [21], and the strength of single crystal γ -TiAl is also lowered by point defect [22]. The resistance of Ti-6Al-4V alloy, which was processed for typical fan blade applications, to high-cycle fatigue in the presence of foreign-object damage was reduced due to earlier crack initiation. The nucleation and subsequent near-threshold growth of crack was primarily affected by the stress concentration associated with the foreign-object damage and the presence of small cracks in the damaged zone. Due to difficulties in observing the dynamic process during deformation with experiments, MD simulation has become an effective method to investigate micro deformation mechanism. Defects such as grain boundary, void and segregation play significant roles in the process of fracture [23]. This paper focus on the evolution of microstructure, tending to find out its connection to cold deformation behavior of two phase TiAl alloy. MD simulation including model creation and analysis method is given in Section 2, Results and discussion are in Section 3.

2. Molecular Dynamics Simulation

2.1. Atomic Potential

The interaction of particles in the material is determined by interatomic potential. Many reported simulation cases of ~~deform-~~ deforming and crack propagation in metal materials were performed

with embedded atomic method due to its better accuracy in metal lattice compare with F-S and L/J [24–26]. Embedded atom method (~~MEAM~~^{MEAM}) potential developed by Zope and Mishin [27] was used in the study. The simulation is performed with the Large-scale Atomic/Molecular Massively Parallel Simulator (LAMMPS) open-source code [28]. We ~~performed~~ ~~did~~ constant-pressure and constant-temperature (NPT) MD simulation at room temperature (298K). Definition of the potential is as following:

$$E_{total} = \sum F_i(\rho_{h,i}) + \frac{1}{2} \sum_i \sum_{j(j \neq i)} \phi_{ij}(R_{ij}) \quad (1)$$

where E_{total} is the total energy of the system, $\rho_{h,i}$ is the host electron density at atom i due to the remaining atoms of the system, $F_i(\rho)$ represents the energy for embedding atom i into the background electron density ρ , and $\phi_{ij}(R_{ij})$ gives the core-core pair repulsion between atoms i and j separated by the distance R_{ij} . It can be noted that F_i only depends on the element of atom i and ϕ_{ij} only depends on the elements of atoms i and j .

2.2. Modeling

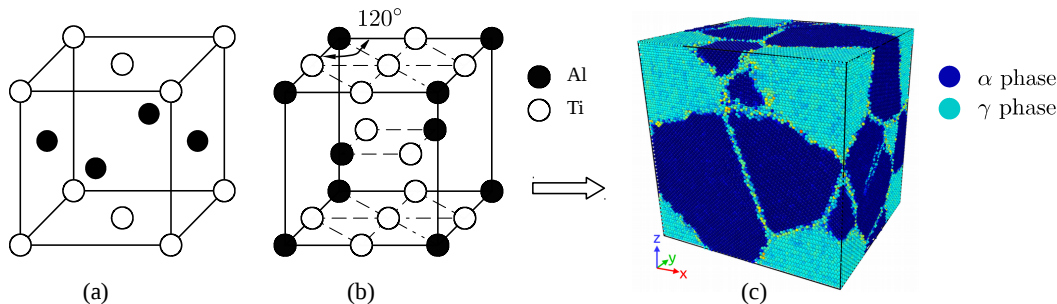


Figure 1. Unit cell of TiAl (a), Ti_3Al (b) and two phase Ti-Al model (c)

Table 1. Parameters of nanocrystalline

Phase	Space group	Designation	Parameters
$\alpha_2 - Ti_3Al$	P6 ₃ /mmc	0 ₁₉	$a = 0.5765$ $c = 0.46833$
$\gamma - TiAl$	tP4	L1 ₀	$a = 0.3997$ $c = 0.4062$

Two phase Ti-Al alloy is composed of γ -TiAl and α_2 - Ti_3Al . ~~TiAl~~ has a fcc type cell with an L1₀ structure, and ~~α_2~~ - Ti_3Al has a hcp structure, these two types of initial cells are shown in Fig. 1. ~~constructing~~. ~~Geometry~~ parameters of the two type of unit cell are given by table 1. Periodic boundary conditions (PBC) ~~are~~ ~~were~~ applied along three directions, which makes polycrystal with periodic nanovoid structures. The initial ~~dimension of simulation cell~~ ~~size of simulation box~~ is $L_x = 200 \text{ \AA}$, $L_y = 180 \text{ \AA}$, $L_z = 210 \text{ \AA}$, and each model ~~contains~~ about 460,000 atoms. The model ~~contains~~ ~~includes~~ 6 grains, with random shape and orientation ~~were created with~~ ~~created by~~ Voronoi method. ~~Uniaxial lead was applied to the model at~~ Total simulation time is restricted to computer power, thus strain rate in molecular dynamic simulation is much greater than physical experiments. Attempts have been done to find decent time step and strain rate for tensile test with MD simulation. If the strain rate is too high and time step is too large in the simulation, the model cannot predict the real behavior of dislocations. Previous work [22,29] reveals that a strain rate of from 10^8 s^{-1} to 10^9 s^{-1} is appropriate for system composed of metal atoms like Ti-Al metallic materials. Thus the strain rate of uniaxial loading was set as $5 \times 10^8 \text{ s}^{-1}$.

2.3. Analysis method

In order to identify typical defects in the deformed model, a hybrid analysis method was used with free code ovlto[2][30]. Dislocation is visualized by DXA method, and centro-symmetry parameter(CSP) is used to differ grain boundaries from α_2 phase grains and γ phase grains. The definition of CSP is as following:

$$P = \sum_{i=1}^6 |\vec{R}_i + \vec{R}_{i+6}|^2 \quad (2)$$

where \vec{R}_i and \vec{R}_{i+6} are the vectors corresponding to the six pairs of opposite nearest neighbors in the fcc lattice. The centro-symmetry parameter(CSP) is zero for atoms in a perfect lattice. In other words, if the lattice is distorted, the value of P will not be zero. Instead, the parameter will have a value within the range corresponding to a particular defect. By removing all the perfect and surface atoms within the bulk, atoms around defected zone are visualized.

2.4. Model Verification

The results of molecular dynamics simulation greatly rely on accuracy of potential and controlling parameters such as strain rate, temperature and relaxation time. Thus we performed model verification on a simplified model and then compared the results with experiments and simulation done by others. uniaxial tensile loading was applied to single crystal γ -TiAl bulk shown

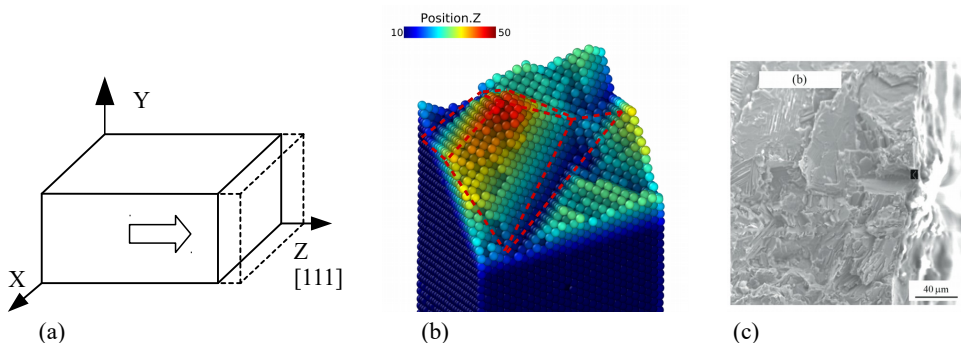
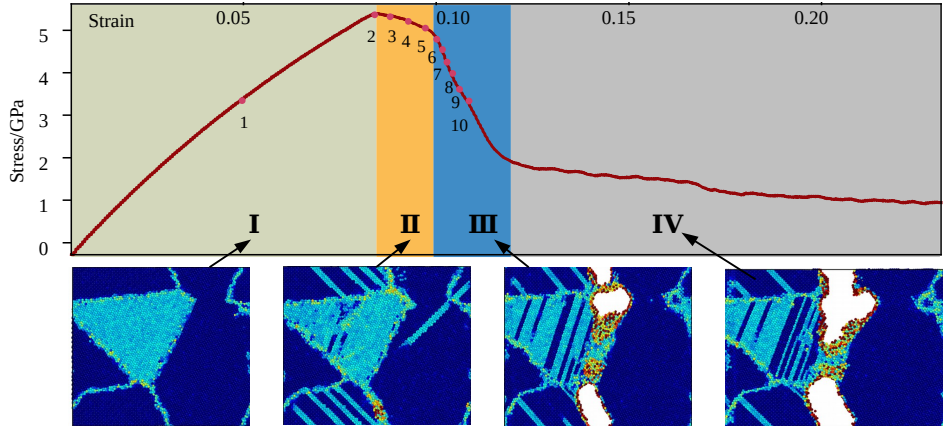


Figure 2. (a) Verifying model: TiAl single crystal bulk (b) Cracked surface of atomic model
(c) Cracked surface from experiment[31]

by Fig. 2(a), potential and relaxation parameters are as same as which applied to the polycrystalline model. When temperature is 300K, the sample was tensioned along [0 0 1] direction at a constant stain rate of 5×10^8 s $^{-1}$. The yield strength of the single crystal TiAl alloy is 9.5 GPa and that is in good agreement with work by Tang[32] in consideration of size effect. And the snapshot of the fracture surface is shown by Fig. 2, and compared with experiment results by Cao[31] shown in Fig. 2(c). It should be noticed that the image from SEM is in a greater scale than our simulation cell. However, the cracked surface in atomic model exhibits two major characteristics of TiAl alloy. First, the fracture type of TiAl at room temperate is typical brittle failure. Second, the fracture surface of atomic model in Fig. 2 (b) is typical cleavage surface. This verification case has proven that the EAM potential is efficiency and accurate enough, and the simulation work flow is valid to predict failure behavior of the system composed of Ti-Al.

3. Results and Discussion

Deformation process of the model without void is shown in Fig. 3. The strength of the model without void is 5.3 GPa. According to stress response under constant rate of strain rate, the whole tensile process can be divided into four stages: stage - I: elastic stage, from $\epsilon = 0$ to $\epsilon = 0.092$, including key point 1, stage - II: yield stage, ranging from $\epsilon = 0.092$ to $\epsilon = 0.101$, including key points 2 to 6, stage

**Figure 3.** Deformation process of the model without void

- III: cracking stage, ranging from $\epsilon = 0.101$ to $\epsilon = 0.112$, including key point 7 to 10, stage - IV: fracture stage. Following discussion concentrates on deformation phenomena that rely on the elasto-plastic codeformation of the γ and α_2 phases and on the particular point defect situation occurred in two phase alloys.

Table 2. Key points during tensile process

Number	1	2	3	4	5	6	7	8	9	10
Stage	I	I	II	II	II	II	III	III	III	III
Strain	0.05	0.088	0.092	0.096	0.099	0.101	0.104	0.107	0.110	0.112

3.1. Deformation Mechanism of Two Phase Ti-Al Alloy

Snapshots of atom During elastic stage, the deformation of α_2 phase and γ phase grains is compatible, however the properties of two phases are different. The elastic constants given by experiments[33,34] are listed in table 3. $C_{11}^{\alpha_2}$ is 176, which is smaller than C_{11}^{γ} , other 5 parameters but C_{33} of Ti_3Al are also smaller than $TiAl$. In order to quantify the difference of the two phase, deformation gradient was calculated by formulation:

$$\mathbf{F}^e = \frac{\partial \mathbf{x}}{\partial \mathbf{X}} = \text{Grad } \mathbf{x}, \quad F_{ij} = \frac{\partial x_i}{\partial X_j} \quad (3)$$

we computes the atomic level elastic strain and deformation gradient tensors in crystalline systems with the numerical method proposed by [11]. When global strain is 0.015, local elastic strain F_{xx} of the model is measured along the line cross center of the model and shown by Fig. 4. In te figure, α_2 phase located in the central part of the axial, and other parts on the axial are γ phase. It should be noticed that atomic level elastic strain effected by random thermal displacements of atoms, thus fluctuation value exists in Fig. 4. The local strain of α_2 phase grain is greater than γ phase grain when global strain of model is 0.015. From the value of local strain we can conclude that γ phase less deformable than α_2 phase during elastic stage.

Table 3. Elastic constants of $TiAl$ and Ti_3Al

	C_{11}	C_{12}	C_{13}	C_{33}	C_{44}	C_{66}
$TiAl$ [33]	186	72	74	176	101	77
Ti_3Al [34]	176	87.8	61.2	218.7	91.9	62.4

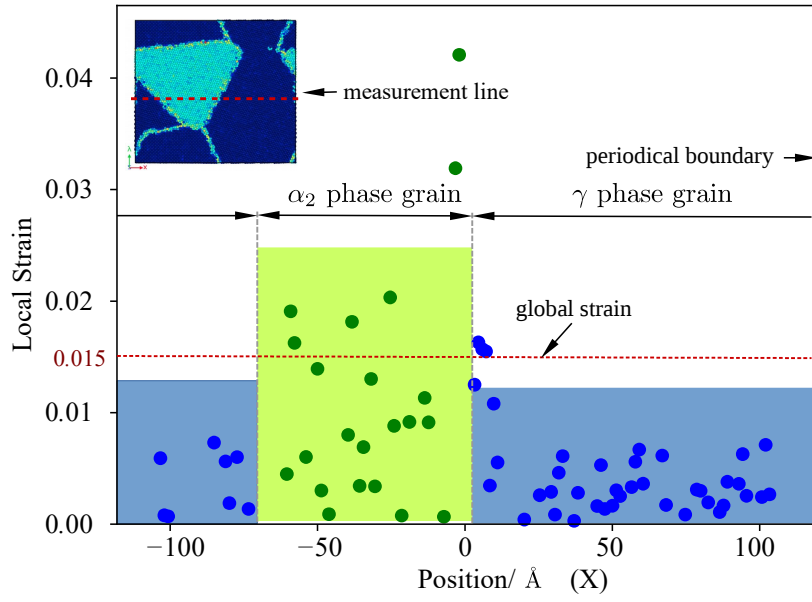


Figure 4. Local strain along tensile direction

Snapshots of atoms configuration at the 3 of 10 key points are shown by Fig. 5. Atoms with ordered configuration of γ phase grains have been removed in Fig. 5(a) and (b), α_2 phase and defects inside grains have been left. Similarly, γ phase grain have been removed in Fig. 5(c) and (d), the defects of α_2 phase have been left. The results show that, at stage I, the structure of material is under typical elastic deformation, the size of simulation box enlarged due to the loading. In this stage, deformation of the two phase are compatible. Emission of dislocation and evolution of defects initiated at the end of stage I. A great number of dislocation emitted inside γ phase at earlier part of stage II, however, the dislocation inside α_2 phase was emitted at the end of stage II is shown by Fig. 5(c). Experiments have

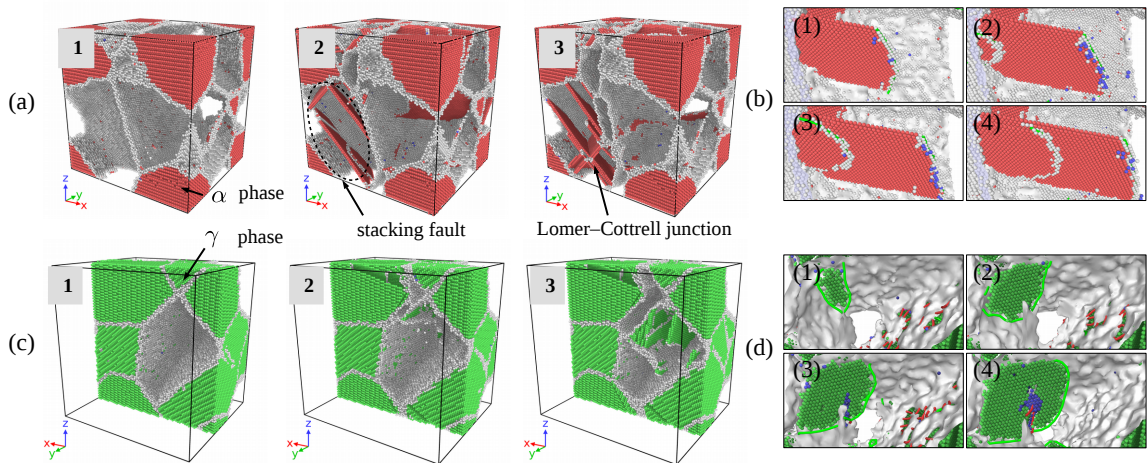


Figure 5. Microstructure evolution inside γ phase(a,b), α_2 phase(c,d) during yield stage

shown that the velocity of dislocation motion is sensitive to stress and temperature[35]. The brittleness of two phase Ti-Al alloy attributed to the poor mobility of dislocation at room temperature. Velocity of a screw dislocation can be estimated by Escaig's elastic model [36], it can be written as:

$$v = v_0 e^{-\Delta H(\tau^*)/kT} \quad (4)$$

where the prefactor v_0 gives the velocity that would be obtained for each potential mobility, L represents the free length of screw character of dislocation, $\Delta H(\tau^*)$ is activation enthalpy determined by loading conditions. The effect of temperature on the mobility can be evaluated under different loading conditions, thus we chose $\tau_1^* > \tau_2^* > \tau_3^*$ in formulation (4), normalized velocity of dislocation motion is shown by Fig. 6. The velocity of dislocation movement rise along with increase of stress, the mobility of dislocation is relatively poor at 298 K. Due to motion of dislocations is inactive inside α_2 phase, typical strengthening mechanism closely related with interaction between grain boundary and dislocation can not be dramatic at room temperature, piling up of dislocations is not observed in this simulation, which is shown in Fig. 5.

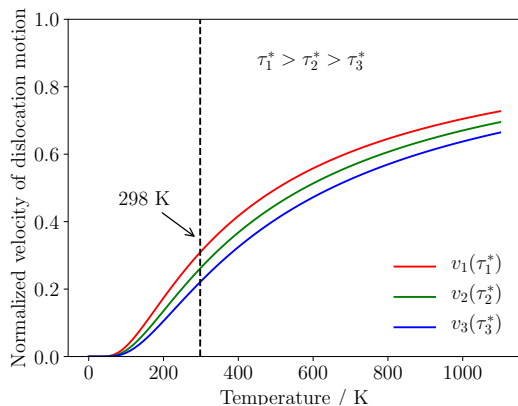


Figure 6. Normalized velocity of dislocation motion under different loading conditions

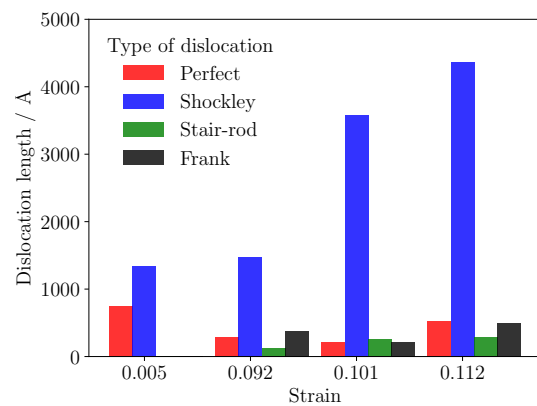
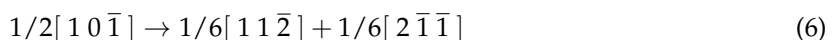
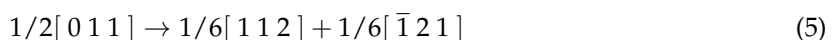
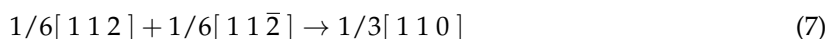


Figure 7. Summary of different types of dislocation under different strain

Length of different types of dislocations are given at four stages in Fig. 7. Dislocations are recognized and identified using the dislocation analysis (DXA) of ovito. The length of Shockley dislocation with Burgers vector $1/6[112]$ increased sharply during yield stage of the deformation process in Fig. 7, but the length of perfect dislocation fluctuated at a low level. Perfect dislocations split into Shockley partial dislocations, this decomposition process can be given by formulation (5) and (6). The structure spontaneously transformed into intrinsic stacking fault (ISF), which can be observed in Fig. 5(a).



Interaction between dislocations with Burgers vector of $1/6[112]$ and $1/6[1\bar{2}\bar{1}]$ follows the decomposition of perfect dislocation. The process produced leading dislocation and trailing dislocation, when the two leading Shockley partials combined, they form Lomer–Cottrell junction, a separate dislocation. It's sessile in the slip plane, playing a role of barrier against other dislocations in the plane. This process is given by :



According to the results calculated by first principle, the stacking fault energy of TiAl is much smaller than Ti_3Al , as a consequence, calculated shear strength of TiAl and Ti_3Al is 4.1 GPa and 2.86 GPa along their easy slip plane respectively[37]. This calculation reveals that tensile behavior in single crystal is mainly controlled by the type of the structure. However, in two phase Ti-Al alloy, deformation of α_2 phase is earlier than γ phase during yield stage, thus local displacement of two phases are incompatible during yield stage. Mobility of dislocation is affected by structure of crystal, loading condition and temperature. And α_2 phase is made up of hcp structured grain, grains with this

type of structure possess less slip system compared with grain with fcc structure [38], thus α_2 phase is difficult do deform under uniaxial tensile loading.

Main reason for the unequal strain partitioning between the α_2 and γ phase is the strong plastic anisotropy of α_2 phase. TEM examinations performed on tensile tested lamellar alloys have revealed that the limited plasticity of α_2 phase is carried by local slip of dislocations with the Burgers vector $1/3[1\bar{1}20]$ prism planes shown by Fig. 5(b), which is by far the easiest slip system in α_2 single crystals. Dislocation neighboring interfaces often needs to be transformed. For example, an ordinary $1/2[110]$ dislocation gliding in one γ grain has to be converted into $[101]$ super dislocation when the double Burgers vectors gliding in an adjacent γ grain. At the α_2/γ interface, dislocations existing in $D0_{19}$ structure transform into dislocations, which is consistent with the $L1_0$ structure. These core transformations are associated with the change of the dislocation line energy because of the differences of the length and the shear module. Pyramidal slip of the α_2 phase is required when slip is forced to cross α_2 phase, this process needs an extremely high shear stress. **Two components(α_2 and γ phase) exhibit different properties in two phase alloy comparing they are single phase alloy respectively.** γ phase is the major source of dislocation in two phase alloy, that is in good agreement with experiments[8,11,39]. When global strain is greater than 0.07, the reason why Ti3Al exhibits less plastic deformation is the absence of twinning in Ti3Al under tensile loading, which have been observed by experiments[5]. The deformation Ti3Al is mainly constrained by loading conditions, as compression loading is applied, Ti3Al activates more moveable dislocation, thus exhibits better elasticity[40].

3.2. The effect of void on the strength of material

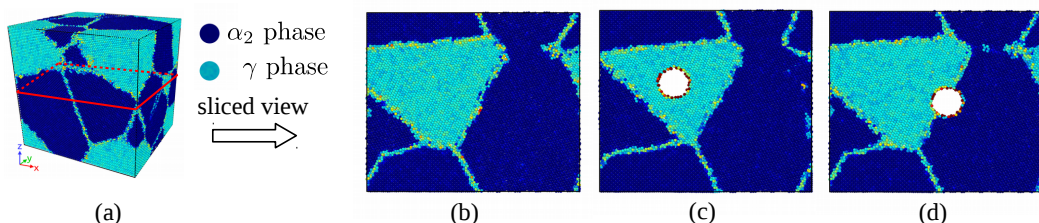


Figure 8. Model of the simulation(a) and sliced view of the model with no void(b), inside α_2 phase(c) at α_2/γ phase boundary(d)

In Fig. 8, voids with different size of 2\AA , 5\AA , 10\AA and 15\AA were placed at α_2/γ phase boundary, inside γ phase respectively. The strength of materials with void in different size and at different position is shown in Fig.9. The existence of void have little impact on the elastic properties of the material, and the model without void has the largest strength 5.3 GPa, the yield stress of model with void is smaller. Void at α_2/γ phase boundary detracts the strength of material most, and the void inside α_2 phase have less impact on the strength. Conventional definition of strength of materials with geometry subtraction was applied to the model, and theoretical strength of the models was calculated by

$$\sigma^* = \sigma_0 \cdot (A^*/A_0) \quad (8)$$

where σ_0 is the strength of model without voids of 5.3 GPa, and A_0 represents initial section area, A^* is effective section area in consideration of the area detraction by void. In classic theory, the relationship between void size and strength of the model is linear. However, simulation results reveals that two phase Ti-Al alloy is sensitive to defect of void. Comparing the strength determined from molecular dynamics simulation and the result4s calculated with formulation (8), it can be seen that the main factor that affects the strength of materials is local behavior of the materials, thus evolution of defects have dramatic influence on the yield and fracture process of the materials.

It has been observed in Fig. 10 that voids detract the strength of materials. The max stress of the simulation cell decreases as the volume of voids increases. It can be seen from Fig. 9, there is a critical

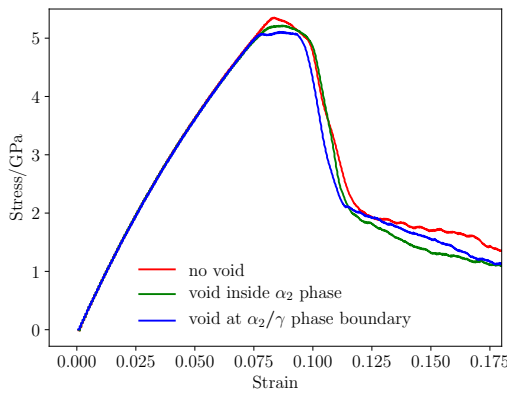


Figure 9. Stress-strain response of the materials under tensile loading

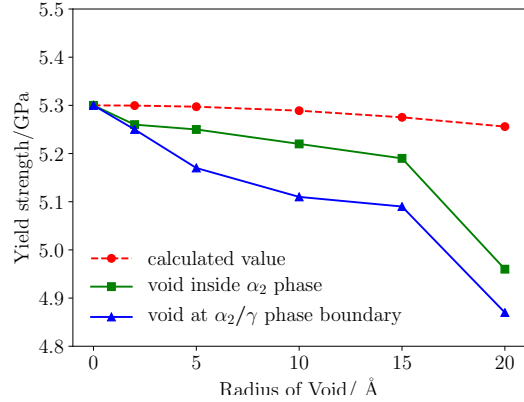


Figure 10. Yield strength of the materials with different size void

value of void radius about 15 Å, the void greater than 15 Å causes serious detraction of strength of material. The decrease rate of loading area are smaller compared with the detraction of strength, so it can be assumed that the yield behavior and strength is more related with local behavior of grain boundaries and void. Grain and phase boundaries are obstacles to deformation process, thus the stability of boundaries have a great impact on the strength of materials. Interactive between grain boundary and void determines the fracture mode of Ti-Al alloy.

3.3. Evolution of spherical void

The role of void can be concluded as two main parts: source of dislocations and obstacles to dislocations, which is dominant depends on the location of void. Void inside α_2 phase plays a role of inclusion, in other words, this type of void possess similar properties as second phase particles.

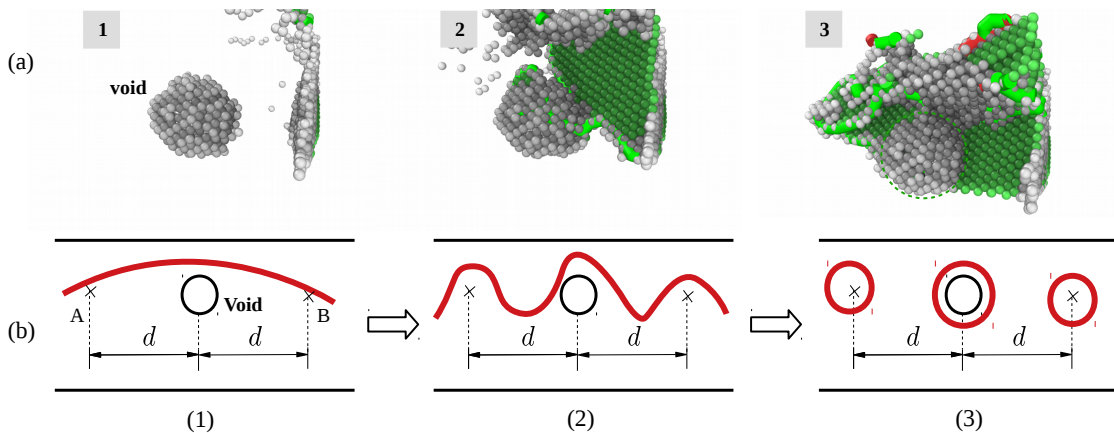


Figure 11. Orowan process occurred inside α_2 phase grain (removed atoms with regular arrangement)

Void inside α_2 phase induced considerable misfit-stress fields and thus can influence material properties. Such stress fields surrounding the second-phase particles can be due to misfit between α_2 phase atoms and surface atoms surrounding the void. That's a possibly favorable effect of second-phase particles that void contribution to the enhancement of mechanical strength. The strengthening effect of the particle inside single phase TiAl alloy has been verified by experiment [41]. Considering yielding of a material as related to glide of dislocations, any mechanism obstructing dislocation glide improves the mechanical strength. The defect evolution neighboring the void during yield stage is shown in Fig. 11(a), the role of void is similar to second-phase particles. It serves as obstacles for dislocation

migration which is shown by Fig. 11(b): the stress fields surrounding the second-phase particles block migrating dislocation, the void particle acts as pinning point. The dislocation can pass two pinning points under shear stress , and the critic value depends on the distance between obstacles, it is be given by [18]:

$$\tau_0 = Gb/d \quad (9)$$

where d represents the distance between two obstacles A and B in Fig. 11 , reflects the dependence of the critical shear stress τ_0 on the second-phase particle density and distribution. This mechanism for hardening is designated as the Orowan process with τ_0 as the Orowan shear stress. As a result of the Orowan process, upon passage of the pinning points by a series of gliding dislocations, a system of concentric loops is formed around the second-phase particles. Consequently, the effective average distance between the second phase particles has decreased to d which implies a necessary increase of the value of critical shear stress required for continuation of dislocation glide. The width of a burgers vector, will be generated at both sides of a crystal along the direction of burgers vector after dislocation traversing the entire crystal, as is shown in the third subfigure of Fig. 11(b).

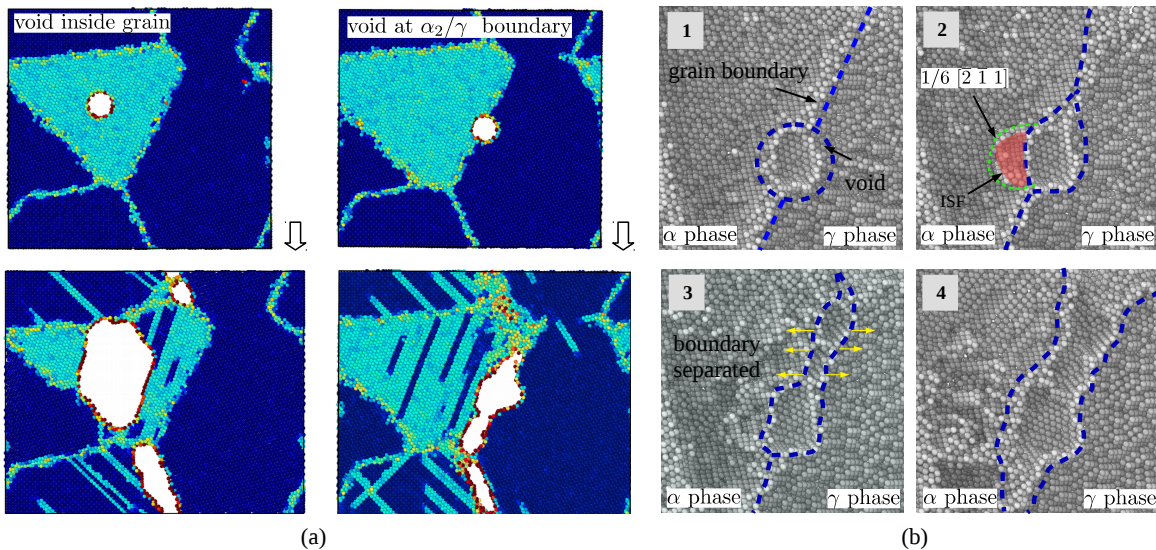


Figure 12. (a) Fracture mode of two types of mode, (b)Evolution of void at α_2/γ phase boundary

Effect of voids at different positions on the crack mode of the material are shown by Fig. 12(a). The model with void fractured cross the grain, and the model with void at α_2/γ boundary resulted a large crack along the boundary under tensile loading. The difference of crack mode can attribute to the position of void and the evolution of the defect. Nucleation, emission of Shockley partial dislocation affect the evolution of the void at boundary greatly due to the anisotropy of two phases on the both sides of the phase boundary. The void weaken the strength of the grain it locates, α_2 phase grain is easy to deformed under shear stress, thus that caused the crack initiated inside grain and finally caused fracture across the grain. Deformation mechanism of the model with void at boundary can be more complex due to the interaction between void and phase boundary. In elastic stage, the system composed of α_2 phase, γ phase and void is in equilibrium, internal stress are balanced under compatible deformation as is shown by the first subfigure of Fig. 12(b). In the middle moment of yield stage, partial dislocation with Burgers vector $1/6[2\bar{1}1]$ emitted from surface of void in Fig. 12(b)-2. The micro crack initialed from the zone neighbor the interface between void and boundary, that quickly caused abrupt decohesion of phase boundary. That accounts for the reason that material with void at α_2/γ phase boundary is weaker than other cases.

4. Conclusion

In this paper, deformation behavior of two phase Ti-Al alloy under tensile loading was simulated with MD method. The mechanism of deformation was investigated under atomic scale, and the effect of void on the properties of two phase Ti-Al alloy was also studied. The conclusions are as follows:

- (1) Major deformation component of the two phase TiAl alloy is Deformation behavior of two types of grain inside $\alpha_2 + \gamma$ two phase Ti-Al alloy are different due to their crystal structure. α_2 phase Ti₃Al grain is easy to be deformed during elastic stage.
- (2) During yield stage, majority of dislocations in two phase TiAl alloy activated inside γ phase, α_2 phase is harder to be deformed slip due to its hcp structure, this inhomogeneity results in cracks at interface of the two phase.
- (3) Effect of void on the strength of the two phase alloy is sensitive to the location of void. Void inside grain has detraction to the strength of material because the strengthening mechanism similar to second phase particle. Void at α_2 / γ boundary is most risky situation for two phase alloy because of fast fracture along boundary.

References

1. Clemens, H.; Mayer, S. Advanced Intermetallic TiAl Alloys. *Materials Science Forum* **2016**, *879*, 113–118, [1006.5010]. doi:10.4028/www.scientific.net/MSF.879.113.
2. Bewlay, B.P.; Nag, S.; Suzuki, A.; Weimer, M.J. TiAl alloys in commercial aircraft engines. *Materials at High Temperatures* **2016**, *33*, 549–559. doi:10.1080/09603409.2016.1183068.
3. Martínková, N.; Nová, P.; Sablina, O.V.; Graphodatsky, A.S.; Zima, J. Karyotypic relationships of the Tatra vole (*Microtus taticus*). *Folia Zoologica* **2004**, *53*, 279–284, [arXiv:1011.1669v3]. doi:10.1007/s13398-014-0173-7.2.
4. Appel, F.; Clemens, H.; Fischer, F.D. Modeling concepts for intermetallic titanium aluminides. *Progress in Materials Science* **2016**, *81*, 55–124. doi:10.1016/j.pmatsci.2016.01.001.
5. Sastry, S.M.L.; Lipsitt, H.A. Plastic deformation of TiAl and Ti₃Al. Proceedings of the 4th International Conference on Titanium, 1980, pp. 1231–1243.
6. Farenc, S.; Coujou, A.; Couret, A. An in situ study of twin propagation in TiAl. *Philosophical Magazine A: Physics of Condensed Matter, Structure, Defects and Mechanical Properties* **1993**, *67*, 127–142. doi:10.1080/01418619308207147.
7. Appel, F. An electron microscope study of mechanical twinning and fracture in TiAl alloys. *Philosophical Magazine* **2005**, *85*, 205–231. doi:10.1080/14786430412331315662.
8. Appel, F.; Wagner, R. Microstructure and deformation of two-phase γ -titanium aluminides. *Materials Science and Engineering R: Reports* **1998**, *22*, 187–268. doi:10.1016/S0927-796X(97)00018-1.
9. Tang, F.L.; Cai, H.M.; Bao, H.W.; Xue, H.T.; Lu, W.J.; Zhu, L.; Rui, Z.Y. Molecular dynamics simulations of void growth in γ -TiAl single crystal. *Computational Materials Science* **2014**, *84*, 232–237. doi:10.1016/j.commatsci.2013.12.014.
10. Kim, Y.W. Effects of microstructure on the deformation and fracture of γ -TiAl alloys. *Materials Science and Engineering A* **1995**, *192-193*, 519–533. doi:10.1016/0921-5093(94)03271-8.
11. Singh, J.B.; Molénat, G.; Sundararaman, M.; Banerjee, S.; Saada, G.; Veysiére, P.; Couret, A. In situ straining investigation of slip transfer across α 2 lamellae at room temperature in a lamellar TiAl alloy. *Philosophical Magazine Letters* **2006**, *86*, 47–60. doi:10.1080/09500830500497066.
12. Hempel, N.; Bunn, J.R.; Nitschke-Pagel, T.; Payzant, E.A.; Dilger, K. Study on the residual stress relaxation in girth-welded steel pipes under bending load using diffraction methods. *Materials Science and Engineering A* **2017**, *688*, 289–300. doi:10.1016/j.msea.2017.02.005.
13. Groh, S.; Marin, E.B.; Horstemeyer, M.F.; Zbib, H.M. Multiscale modeling of the plasticity in an aluminum single crystal. *International Journal of Plasticity* **2009**, *25*, 1456–1473. doi:10.1016/j.ijplas.2008.11.003.
14. Trout, P.E. Plastic Contaminants: Bad News for the Paper Recycler. *Tappi* **1972**, *55*, 956–958. doi:10.1016/j.cma.2018.06.026.

15. Xu, S.Z.; Hao, Z.M.; Su, Y.Q.; Yu, Y.; Wan, Q.; Hu, W.J. An analysis on nanovoid growth in body-centered cubic single crystalline vanadium. *Computational Materials Science* **2011**, *50*, 2411–2421. doi:10.1016/j.commatsci.2011.03.019.
16. Jing, P.; Yuan, L.; Shivpuri, R.; Xu, C.; Zhang, Y.; Shan, D.; Guo, B. Evolution of spherical nanovoids within copper polycrystals during plastic straining: Atomistic investigation. *International Journal of Plasticity* **2018**, *100*, 122–141. doi:10.1016/j.ijplas.2017.09.016.
17. Elkhatib, M.G.; Shin, Y.C. Molecular dynamics-based cohesive zone representation of Ti6Al4V/TiC composite interface. *Materials and Design* **2018**, *155*, 161–169. doi:10.1016/j.matdes.2018.05.054.
18. Xiong, L.; Xu, S.; McDowell, D.L.; Chen, Y. Concurrent atomistic-continuum simulations of dislocation-void interactions in fcc crystals. *International Journal of Plasticity* **2015**, *65*, 33–42. doi:10.1016/j.ijplas.2014.08.002.
19. Kiener, D.; Hosemann, P.; Maloy, S.A.; Minor, A.M. In situ nanocompression testing of irradiated copper. *Nature Materials* **2011**, *10*, 608–613. doi:10.1038/nmat3055.
20. Yang, Y.; Baker, I. The influence of vacancy concentration on the mechanical behavior of Fe-40Al. *Intermetallics* **1998**, *6*, 167–175. doi:10.1016/S0966-9795(97)00062-9.
21. Nazmy, M.; Staubli, M.; Onofrio, G.; Lupinc, V. Surface defect tolerance of a cast TiAl alloy in fatigue. *Scripta Materialia* **2001**, *45*, 787–792. doi:10.1016/S1359-6462(01)01097-1.
22. Brimmo, A.T.; Hassan, M.I.; Shatilla, Y. Transient heat transfer computational model for the stopped aluminium reduction pot - Cooling techniques evaluation. *Applied Thermal Engineering* **2014**, *73*, 114–125. doi:10.1016/j.applthermaleng.2014.07.011.
23. Larsen, P.M.; Schmidt, S.; SchiØtz, J. Robust structural identification via polyhedral template matching. *Modelling and Simulation in Materials Science and Engineering* **2016**, *24*, 055007, [1603.05143]. doi:10.1088/0965-0393/24/5/055007.
24. Ko, W.S.; Grabowski, B.; Neugebauer, J. Development and application of a Ni-Ti interatomic potential with high predictive accuracy of the martensitic phase transition. *Physical Review B - Condensed Matter and Materials Physics* **2015**, *92*, 134107. doi:10.1103/PhysRevB.92.134107.
25. Zepeda-Ruiz, L.A.; Stukowski, A.; Oppelstrup, T.; Bulatov, V.V. Probing the limits of metal plasticity with molecular dynamics simulations. *Nature* **2017**, *550*, 492–495. doi:10.1038/nature23472.
26. Fan, H.; Zhu, Y.; El-Awady, J.A.; Raabe, D. Precipitation hardening effects on extension twinning in magnesium alloys. *International Journal of Plasticity* **2018**, *106*, 186–202. doi:10.1016/j.ijplas.2018.03.008.
27. Zope, R.R.; Mishin, Y. Interatomic potentials for atomistic simulations of the Ti-Al system. *Physical Review B - Condensed Matter and Materials Physics* **2003**, *68*, 024102, [arXiv:cond-mat/0306298]. doi:10.1103/PhysRevB.68.024102.
28. Plimpton, S. Fast parallel algorithms for short-range molecular dynamics. *Journal of Computational Physics* **1995**, *117*, 1–19, [arXiv:10.1002/nag.2347]. doi:10.1006/jcph.1995.1039.
29. Zhu, T.; Li, J.; Samanta, A.; Leach, A.; Gall, K. Temperature and strain-rate dependence of surface dislocation nucleation. *Physical Review Letters* **2008**, *100*, 025502. doi:10.1103/PhysRevLett.100.025502.
30. Stukowski, A. Visualization and analysis of atomistic simulation data with OVITO-the Open Visualization Tool. *Modelling and Simulation in Materials Science and Engineering* **2010**, *18*, 015012, [arXiv:10.1002/nag.2347]. doi:10.1088/0965-0393/18/1/015012.
31. Chen, J.H.; Cao, R. Chapter 9 - Brittle Fracture of TiAl Alloys and NiTi Memory Alloys. In *Micromechanism of Cleavage Fracture of Metals*; Chen, J.H.; Cao, R., Eds.; Butterworth-Heinemann: Boston, 2015; pp. 365–443. doi:<https://doi.org/10.1016/B978-0-12-800765-5.00009-5>.
32. Tang, T.; Kim, S.; Horstemeyer, M.F. Molecular dynamics simulations of void growth and coalescence in single crystal magnesium. *Acta Materialia* **2010**, *58*, 4742–4759. doi:10.1016/j.actamat.2010.05.011.
33. He, Y.; Schwarz, R.; Migliori, A.; Whang, S. Elastic constants of single crystal γ -TiAl. *Journal of Materials Research* **1995**, *10*, 1187–1195. doi:10.1557/JMR.1995.1187.
34. Tanaka, K.; Okamoto, K.; Inui, H.; Mlonishl, Y.; Yamaguchi, M.; Koiwa, M. Elastic constants and their temperature dependence for the intermetallic compound Ti3Al. *Philosophical Magazine A: Physics of Condensed Matter, Structure, Defects and Mechanical Properties* **1996**, *73*, 1475–1488. doi:10.1080/01418619608245145.
35. Stein, D.F.; Low, J.R. Mobility of edge dislocations in silicon-iron crystals. *Journal of Applied Physics* **1960**, *31*, 362–369. doi:10.1063/1.1735574.

36. Escaig, B. L'activation thermique des déviations sous faibles contraintes dans les structures h.c. et c.c. Par. *Physica Status Solidi (B)* **1968**, *28*, 463–474. doi:10.1002/pssb.19680280203.
37. Liu, Y.L.; Liu, L.M.; Wang, S.Q.; Ye, H.Q. First-principles study of shear deformation in TiAl alloys. *Journal of Alloys and Compounds* **2007**, *440*, 287–294. doi:10.1016/j.jallcom.2006.09.027.
38. Rösner, H.; Markmann, J.; Weissmüller, J. Deformation twinning in nanocrystalline Pd. *Philosophical Magazine Letters* **2004**, *84*, 321–334. doi:10.1080/09500830410001675687.
39. Singh, J.B.; Molénat, G.; Sundararaman, M.; Banerjee, S.; Saada, G.; Veyssiére, P.; Couret, A. In situ straining investigation of slip transfer across α 2 lamellae at room temperature in a lamellar TiAl alloy. *Philosophical Magazine Letters* **2006**, *86*, 47–60. doi:10.1080/09500830500497066.
40. habil. Fritz Appel, D.; Paul, D.J.D.H.; Oehring, D.M.; Microstructures, L. Deformation Behavior of Two-Phase α_2 (Ti₃Al) + γ (TiAl) Alloys. *Gamma Titanium Aluminide Alloys* **2011**, *2*, 125–248. doi:10.1002/9783527636204.ch6.
41. Zghal, S.; Menand, A.; Couret, A. Pinning points anchoring ordinary and shockley dislocations in TiAl alloys. *Acta Materialia* **1998**, *46*, 5899–5905. doi:10.1016/S1359-6454(98)00233-X.

Funding: This research was funded by the National Natural Science Foundation of China (No.51665030, No.51865027) and the Program for Changjiang Scholars and Innovative Research Team in Universities of the Ministry of Education of China (No. IRT-15R30), the Hongliu First-class Disciplines Development Program of Lanzhou University of Technology.

Acknowledgments: Fig.2(c) is from Chen, J.H.; Cao, R. Chapter 9 - Brittle Fracture of TiAl Alloys and NiTi Memory Alloys. In *Micromechanism of Cleavage Fracture of Metals*; Chen, J.H.; Cao, R., Eds.; Butterworth-Heinemann: Boston, 2015; pp. 365–443. Author have get permission from publisher. License number:4492240737073

© 2018 by the authors. Submitted to *Materials* for possible open access publication under the terms and conditions of the Creative Commons Attribution (CC BY) license (<http://creativecommons.org/licenses/by/4.0/>).